Portable Embedded System for Contactless Measurement of Material Conductivity

Nuno Francisco Medeiros Rodrigues
Instituto de Telecomunicações, Instituto Superior Técnico,
Av. Rovisco Pais 1, 1049-001 Lisboa, Portugal
nuno.medeiros.rodrigues@tecnico.ulisboa.pt

***Abstract* – Non-Destructive Testing (NDT) of metallic materials such as aluminium is a growing area that requires novel sensing solutions. From the several NDT methods, eddy currents testing is the preferred to inspect metallic parts and welding joints searching for flaws and other material discontinuities. Eddy currents sensors are devices capable of contactless assessment with high-resolution measurements of any conductive target. High resolution and tolerance in dirty environments make eddy currents sensors indispensable in modern industrial operations.**
One of the uses of eddy currents sensors is to measure electrical conductivity. The value of the electrical conductivity of a metal depends on its chemical composition and crystalline structure. This work presents the development, implementation and characterization of a compact embedded system for contactless metal conductivity measurements.

***Keywords* – Non-Destructive Test, Eddy Current Testing, Metal Conductivity, Contactless, Digital Signal Processing, Embedded System.**

I. INTRODUCTION

There are many types of NDT techniques based on eddy currents, ultrasound, induction, magnetic flux leakage, Electromagnetic Acoustic Transducer and other physical principles. These methods allow to test materials, components and systems without limiting future usability and, sometimes, disassembling the parts under test from their original location. NDT probes and sensors use many different technologies, but often consist of ultrasonic, eddy current, or corrosion-detection devices. Typically, these NDT products are used to perform acoustic emission testing, interferometry, leak testing, magnetic particle testing, radiographic testing, or computed tomography [1].

Some probes and sensors use electromagnetic comparators to sort components that are manufactured with different metals. Electromagnetic comparators use coils where an AC current is applied. When a metal part is brought close to the coil, the coil impedance is affected. These probes and sensors compare the amplitude, phase, and harmonic distortion of the output voltage to determine component composition.

Since 1950, Eddy Current Testing (ECT) has developed increasingly in materials testing, especially in the aircraft and nuclear industries. The extensive research and development [2] in highly sensitive sensors and instruments over the last years indicates that ECT is a widely used inspection technique and its increased applicability is ongoing.

Electrical Conductivity is the ability of a material to transfer electric current. It is the reciprocal of electrical resistivity Ω. Its SI derived unit is the Siemens per meter (S/m), but conductivity values are often reported as percent IACS. This property is very useful since values are affected by such things as the substances chemical composition and the stress state of crystalline structures. Therefore, electrical conductivity information can be used for measuring the purity of water, sorting materials, checking for proper heat treatment of metals, and inspecting for heat damage in some materials.

The main objective of this work is to develop a miniaturized handheld contactless electrical conductivity measurement system based on eddy currents. As such, the goals of this project are to develop: (i) an embedded measurement system: (ii) firmware capable of performing the signal processing necessary for the estimation of impedance sensor (coil) phasor; (iii) communication with the terminal; (iv) program a graphical user interface to present results; (v) make measurements of various conductivity samples and (vi) implement methodologies for correction/conductivity measurement calibration.

II. RELATED RESULTS IN THE LITERATURE

Eddy currents sensors operate with magnetic fields. A driver creates an alternating current in a coil which in turn generates an alternating magnetic field that induces eddy currents in the target material. The eddy currents create an opposing magnetic field which resists the field being generated by the probe coil [3]. The interaction of the magnetic fields is dependent on the distance between the probe and the target material and also on the actual material composition. If the distance between the coil and the material changes, the electronic measurement system senses the change in the field interaction (either thru the same coil or another sensing coil) and produces a voltage

output that depends on the change in distance between the probe and target [4]. When the material target changes there is also a change in the field interaction that produces a change in the voltage output. These effects will make it possible to distinguish between different materials.

If the eddy current measurement circuit is somehow balanced in air and then placed on a piece of material, the resistance component will increase (eddy currents are being generated in the material and this takes energy away from the coil, which shows up as resistance) and the inductive reactance of the coil decreases (the magnetic field created by the eddy currents opposes the coil's magnetic field and the net effect is a weaker magnetic field) [5].

Thicknesses of non-metallic coatings on metal substrates can be determined simply from the effect of lift-off on the sensor output. Lift-off is the distance between the inspection coil probe and the test piece. Lift-off variations can be caused by varying coating thickness, irregular sample surfaces or the operator's movement [6]. When the probe is closer to the target, eddy currents are stronger as represented in Fig. 1.

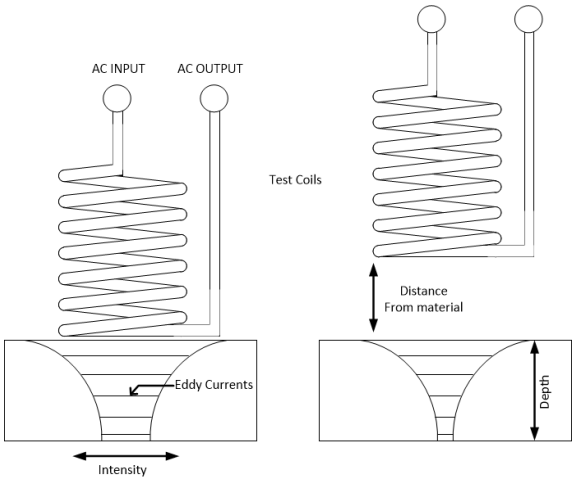

Fig. 1. Lift-off effect. When the probe is closer to the target, eddy currents are stronger.

Eddy current sensors for use in precision displacement measurement and metrology applications [7] use complex electronic designs for driving the probes and measuring their outputs. These high-performance sensors have outputs which are very linear, stable with temperature, and able to resolve small changes in target position.

In the literature [8] there are equations that allow to reach an estimate of the real and imaginary part of the measured signal from a known lift-off and conductivity. The theoretical result for a frequency of 63.3 kHz with a 1 mm radius and length coil is show in Fig. 2. Each letter represents a metal with different conductivity and lift-off characteristics. Table 1 has the electrical conductivity (σ) and relative magnetic permeability (μ_R) of each sample.

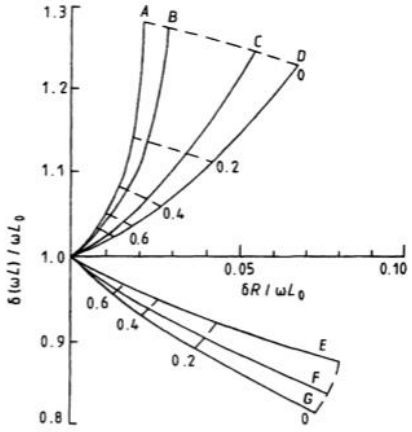

Fig. 2. Theoretical result of variations of $\delta(\omega L)/\ \omega L_0$ and $\delta R/\omega L_0$ from balance position at 'infinite' lift-off plotted versus height of lift-off in millimeters for a surface-scanning coil. The coil radius and length are 1 mm*. Each letter represents a metal with different conductivity and permeability [8].*

Table 1. Electrical conductivity (σ) and relative magnetic permeability (μ_R) of each metal used in the simulation.

	σ (MS/m)	σ (%IACS)	μ_R
A	1	1.67	100
B	1	1.67	50
C	10	16.7	100
D	10	16.7	50
E	20	33.3	1
F	40	66.7	1
G	60	100	1

III. MEASUREMENT SYSTEM DESCRIPTION

The objective of this project is to develop a small handheld system to perform contactless conductivity measurements when attached to a portable device. In the proposed architecture, the measurement system generates synchronous sine signals using two Direct Digital Synthesizer (DDS), one is software implemented in the dsPIC microcontroller (dsPIC33EP256MU806) and the other is hardware implemented. The external DDS will have at its output one sine wave that will be used to stimulate the probe AC current. The probe is a bridge where each arm is an RL series circuit. One of the inductances generates the magnetic field in the material under test, while the other coil is identical but is placed

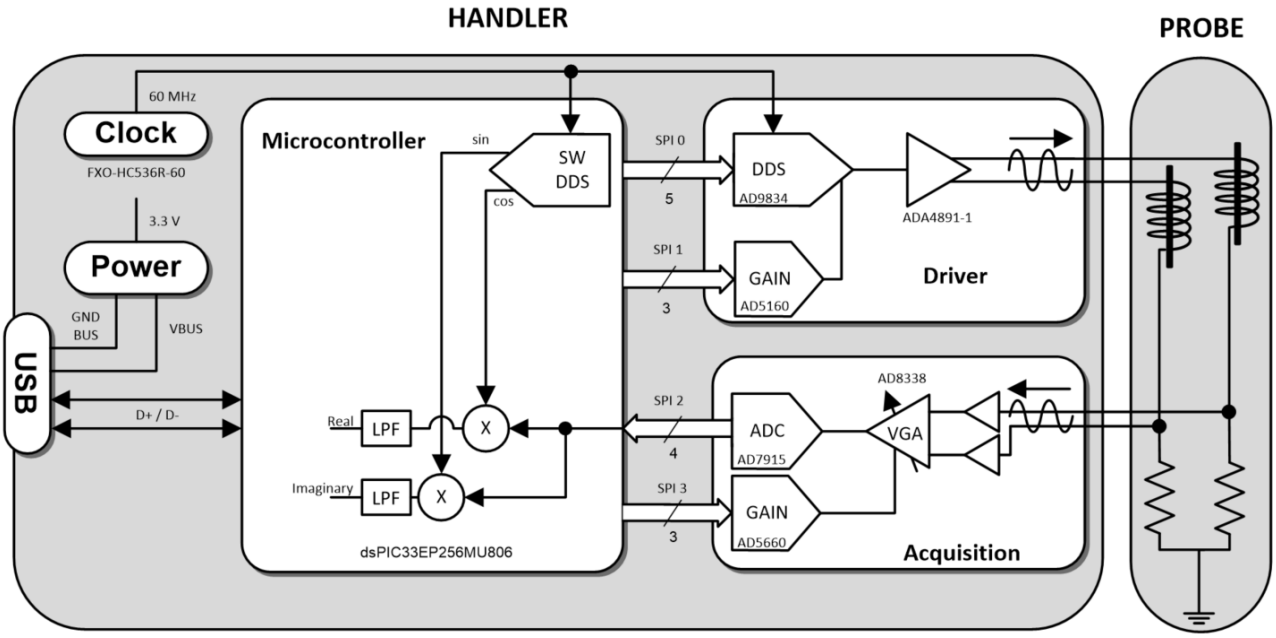

Fig. 4. Block diagram.

away from the material. The bridge output is amplified by a Variable Gain Amplifier (VGA) before it is digitized with a single Analog-to-Digital Converter (ADC). This voltage has a phase shift and different amplitude when compared with the stimulus signal but the same frequency. After the ADC conversion, the samples will be processed in the microcontroller. This signal processing includes heterodyning the acquired signal with the two internal DDSs to obtain the in-phase and in-quadrature components of the measured signal. From these two components, the system estimates the electrical conductivity of the material and the probe lift-off. The complete system block diagram is shown in Fig. 4.

The final version of the system (with its casing) with a mini-USB interface is shown in Fig. 3

Fig. 3. Final version of the working system.

A. Driver

To stimulate the probe, the sine wave synthesized in the DDS (AD9834) is used. In this DDS, a sine wave with an output frequency up to 37.5 MHz can be generated. After the DDS, a filter removes the images that are centered at multiple frequencies of the sampling frequency, (60 MHz), and the DC component from the DDS. This bandpass filter is dimensioned to allow frequencies from 1 kHz up to 1 MHz. The sine amplitude is controlled with a digital potentiometer (AD5160) to enable a further degree of control in the driver block without degrading the DDS amplitude resolution. The final element in the driver is a high-speed rail-to-rail amplifier (ADA4891-A) which will supply the current into the probe bridge circuit.

B. Probe

Absolute probes [9] generally have a single coil that generates eddy currents and senses changes in the eddy currents. Absolute probes provide an absolute voltage signal and can be used for flaw detection, conductivity measurements, lift-off measurements and thickness measurements. These probes may have a voltage compensation using an additional reference coil that is far from the inspected material. This setup improves the measurement method since the bridge output voltage only appears when the bridge arms become unbalanced, because when the probe is far from the test sample, both coils have the same impedance and thus the bridge output voltage is null. The probe configuration that is used in this project is shown in Fig. 5.

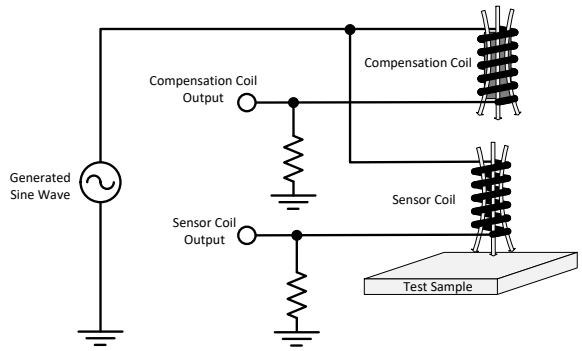

Fig. 5. Configuration of the absolute probe with compensation.

C. Acquisition

The acquisition channel consists on the VGA (AD8338) and on the ADC (AD7915). The VGA differential input suits the bridge measurement setup. However, since the VGA input impedance is relatively low (500 Ω), two amplifiers as buffers are used (AD8028). Notice that the sensor signals have a considerable DC component set by driver (an option made to simplify power management and input biasing on the whole system that uses a single unipolar DC power source), so it is possible to use buffers without adding any additional DC components. The VGA gain is controlled by a programmable DAC (AD5660). After the VGA, the ADC is fully differential input with 16-bit resolution and is capable of up to 1 MS/s.

D. Signal Processing

After acquiring the amplified probe output signal, signal processing enables the estimation of the desired material parameters. The real and imaginary components of the acquired signal are obtained by demodulating the acquired signal with the internal DDS signals. The internal software DDS computes a sine and cosine with the same frequency of the sine produced with the external DDS (AD9834) taking into account that the external DDS operates at 60 MHz and the internal SW DDSs must operate the sampling frequency at which the ADC operates. The necessary synchronization is controlled by setting a deterministic delay between the external DDS start-up and the start of the first ADC conversion. To get the average value of the multiplied signals, the result of the multiplication passes through lowpass IIR (Infinite Impulse Response) filters. The outputs of the multipliers and the filters are

$$\overline{\mathrm{X_{Re}}} = \frac{V_{probe}V_{ref}}{2}\cos\left(\theta_{probe}-\theta_{ref}\right), \quad (1)$$

$$\overline{\mathrm{X_{Im}}} = \frac{V_{probe}V_{ref}}{2}\sin\left(\theta_{probe}-\theta_{ref}\right), \quad (2)$$

where V_{probe} and θ_{probe} are the amplitude and phase of the acquired signal (i.e., the amplified probe output). V_{ref} and θ_{ref} are the known amplitude and phase of the internal SW DDS. From these two components, the magnitude and phase can be obtained.

E. Communication

To communicate between the host device and the dsPIC a datapacket structure was defined as in Table 2.

Table 2. Datapacket structure to send instructions to dsPIC.

Command Type	Size	Data
1 byte	4 bytes	Variable size

Command type is a character that defines the operation between the two devices. From the host device to the dsPIC instructions to program the peripherals or to begin the system processing are sent. To program the peripherals, signal frequency and phase, timer prescale, to define the sampling frequency and the number of acquisitions are sent.

To send the data to the Host program segmented packets as defined in Table 3. This segmentation is required/used when sending large amounts of data.

Table 3. Received data buffer structure.

Message Code	Number of Packets	Packet Index	Packet Payload	Data
1 byte	1 byte	1 byte	2 bytes	Variable size

The packet has an identification field that specifies what kind of data is sent. The packet contains a size field that specifies the amount of data in the packet. For data larger than the maximum packet size, the data is split into different packets and an identifier is used to specify the data order.

F. Interface

To debug the connection between the dsPIC and the host of the application, a Matlab and a labVIEW program is used, but the final interface is in labVIEW. The idea of the host interface is to control the signal characteristic and to display the measured conductivity and a lift-off. Fig. 6 shows the GUI of the labVIEW application.

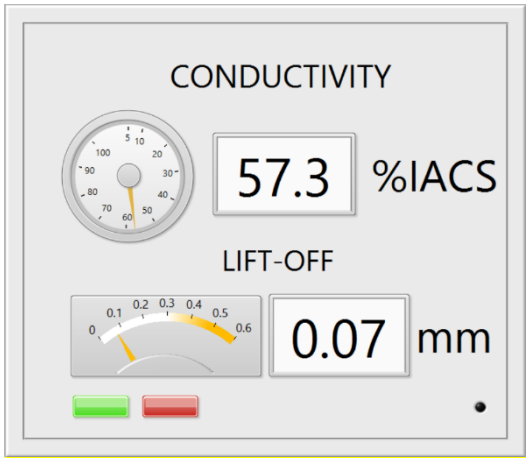

Fig. 6. labVIEW interface for conductivity and lift-off measures.

IV. MEASURED RESULTS

When a target material approaches the probe, it produces a voltage output that depends on the material conductivity, so, it is possible to sort different materials. Fig. 7 shows the histogram of the normalized real and imaginary components of the processed signal for three different materials. In this case, the real component of copper and aluminium are similar, but there is a significant difference in the imaginary component.

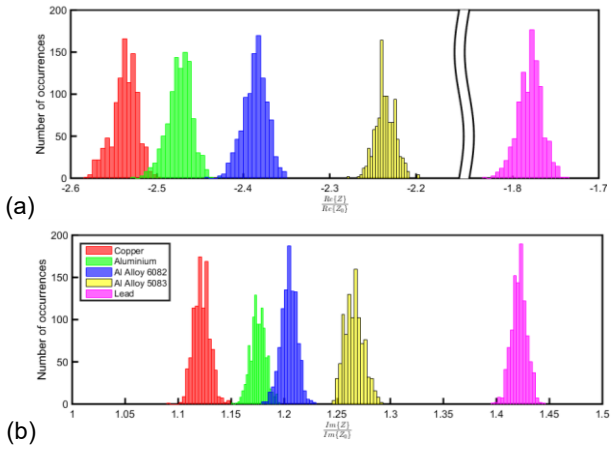

Fig. 7. Histogram of the real (a) and imaginary (b) outputs varying the tested materials with 1000 repetitions, without lift-off and a frequency of 30 kHz.

In Table 4 the mean and standard deviation values of the real, imaginary, magnitude and phase components obtained with 1000 repetitions are shown. The tested materials characteristics are shown in Table 5.

Table 4. Mean and standard deviation values of the real, imaginary, magnitude and phase components obtained with 1000 repetitions.

	Cu	Al	Al 6082	Al 5083	Pb
$\overline{X_{Re}}$	-2.54	-2.47	-2.39	-2.24	-1.78
$\frac{\sigma(X_{Re})}{\overline{X_{Re}}}[\%]$	0.573	0.567	0.582	0.507	0.793
$\overline{X_{Im}}$	1.12	1.18	1.20	1.27	1.42
$\frac{\sigma(X_{Im})}{\overline{X_{Im}}}[\%]$	0.673	0.598	0.625	0.692	0.503
$\overline{\lvert X\rvert}$	1.66	1.66	1.64	1.61	1.53
$\frac{\sigma(\lvert X\rvert)}{\overline{\lvert X\rvert}}[\%]$	0.411	0.385	0.383	0.373	0.405
$\overline{\arg(X)}[^o]$	-87.8	-85.9	-84.2	-81.0	-71.2
$\sigma(\arg(X))[^o]$	0.256	0.247	0.264	0.266	0.278

Table 5 - Conductivity of the materials tested.

	Cu	Al	Al 5083	Al 5083	Pb
σ (%IACS)	100.83	56.4	43.29	28.7	8.25

The output components change with the distance between the probe and the target material. Fig. 8 shows the different output for five materials where the distance between the probe and the target is varying. It is shown, in Fig. 8, that different materials at different lift-off values from the probe exhibit a specific phase and module value, so, it is possible to distinguish between different materials and different lift-off values. Fig. 9 shows the same results but with the real and imaginary components of the signal.

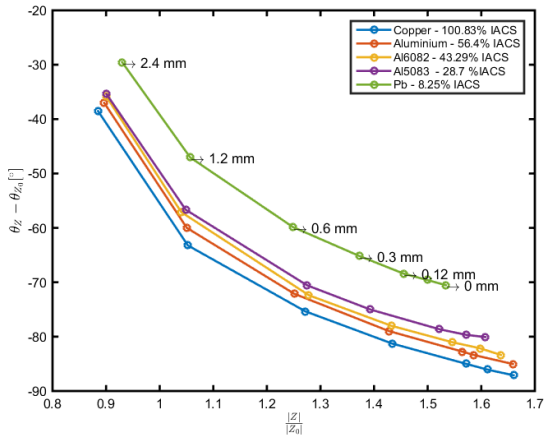

Fig. 8. Normalized phase and magnitude output with different distances between the material under test and the probe. Z_0 is the system measurement when the probe is far from the test sample.

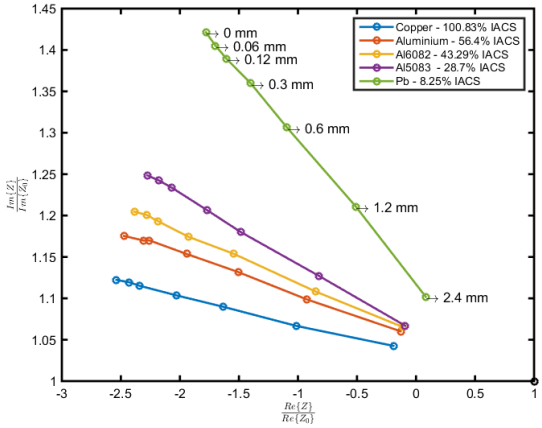

Fig. 9. Normalized real and imaginary outputs with different distances between the material under test and the probe. Z_0 is the system measurement when the probe is far from the test sample.

In theory it is possible to achieve the real and imaginary part from the lift-off and the conductivity of a material [8]. Since the system acquires the real and imaginary part of the signal, it should be possible to estimate the conductivity and lift-off using this relation. A program that generates the results of Fig. 2 solution for different conductivities and lift-offs was made and the result is shown in Fig. 10.

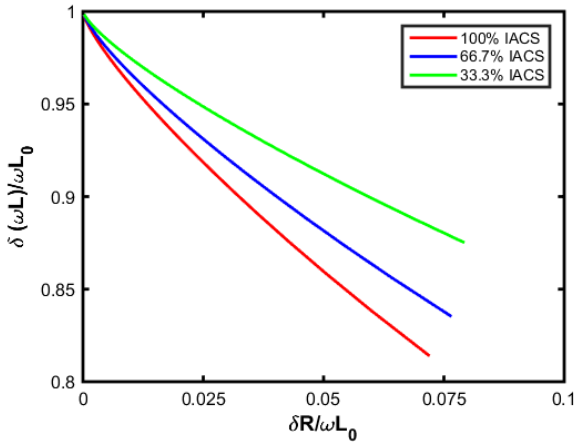

Fig. 10. Simulation of the theoretical predictions of variations of $\delta\omega L/\omega L_0$ and $\delta R/\omega L_0$.

A fit with the measured values to obtain an estimation of the conductivity and lift-off based on those measurements was done.

To estimate the conductivity and lift-off of non-magnetic samples, polynomial functions are used. A third degree polynomial with a coefficient of determination, r^2, of 0.995 to estimate samples conductivity is

$$\begin{aligned}\sigma = {} & p_{00} + p_{10}\,\mathrm{Re(Z)} + p_{01}\,\mathrm{Im(Z)} + p_{20}\,\mathrm{Re(Z)}^2 \\ & + p_{11}\,\mathrm{Re(Z)}\,\mathrm{Im(Z)} + p_{02}\,\mathrm{Im(Z)}^2 + p_{30}\,\mathrm{Re(Z)}^3 \\ & + p_{21}\,\mathrm{Re(Z)}^2\,\mathrm{Im(Z)} + p_{12}\,\mathrm{Re(Z)}\,\mathrm{Im(Z)}^2 \\ & + p_{03}\,\mathrm{Im(Z)}^3\end{aligned}, \quad (3)$$

where coefficient values are listed in Table 6.

Table 6 – Coefficient values of the conductivity polynomial fit.

p_{00}	-5.39×10^{2}	p_{02}	–6.90
p_{10}	-1.10×10^{4}	p_{30}	-5.58×10^{3}
p_{01}	-2.51×10^{2}	p_{21}	-3.48×10^{2}
p_{20}	-8.25×10^{2}	p_{12}	–9.28
p_{11}	-3.33×10^{2}	p_{03}	-9.42×10^{-2}

To estimate the distance between the probe and the material another fit is used. The third degree polynomial with a r^2 of 0.995 to estimate the distance between the coil and the target material is

$$\begin{aligned}d = {} & p_{00} + p_{10}\,\mathrm{Re(Z)} + p_{01}\,\mathrm{Im(Z)} + p_{20}\,\mathrm{Re(Z)}^2 \\ & + p_{11}\,\mathrm{Re(Z)}\,\mathrm{Im(Z)} + p_{02}\,\mathrm{Im(Z)}^2 + p_{30}\,\mathrm{Re(Z)}^3 \\ & + p_{21}\,\mathrm{Re(Z)}^2\,\mathrm{Im(Z)} + p_{12}\,\mathrm{Re(Z)}\,\mathrm{Im(Z)}^2 \\ & + p_{03}\,\mathrm{Im(Z)}^3\end{aligned}, \quad (4)$$

where the coefficient values are listed in Table 7

Table 7. Coefficient values of the lift-off polynomial fit.

p_{00}	1.46×10^{1}	p_{02}	2.18×10^{-03}
p_{10}	-1.38×10^{1}	p_{30}	2.00
p_{01}	2.07×10^{-1}	p_{21}	1.80×10^{-1}
p_{20}	5.08	p_{12}	3.39×10^{-3}
p_{11}	-6.18×10^{-2}	p_{03}	3.31×10^{-5}

With this fitting coefficients a maximum absolute error of 0.04 mm for lift-off and 1.5% IACS for electrical conductivity were achieved. Fig. 11 shows the lift-off absolute error and Fig. 12 shows the electrical conductivity absolute error for five different conductivity samples with different lift-offs. In Fig. 11 the higgest lift-off absolute error was obtained in a sample with 42% IACS and a lift-off of 0.3 mm.

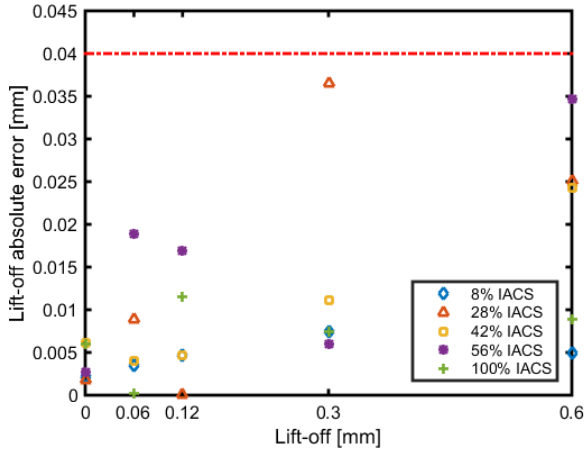

Fig. 11. Lift-off absolute errors.

In Fig. 12 the highest electrical conductivity absolute error was obtained for a sample with 28% IACS and a lift-off of 0.3 mm.

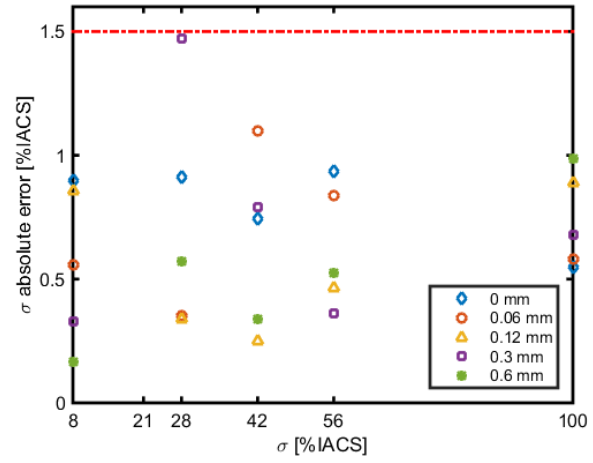

Fig. 12. Conductivity absolute errors.

V. CONCLUSIONS

Eddy currents based NDT systems are one of the most used today to inspect metallic parts in searching for flaws and other material discontinuities. This is because it is a quick, simple, and reliable inspection technique to detect surface and near-surface defects in conductive material. It can be used also to measure material electrical conductivity and non-conductive coating thickness. Currently, this technique is quite evolved and there are some portable options in the market which are ideal for technicians inspecting installed parts.

In this project a special importance on the system size is given. The system is as small as possible to be portable. Its pen-like casing dimensions which can be easily handled by technician. The final system size is 110 × 20 × 15 mm with the 3D printed case included.

The host interface controls and presents the estimated conductivity and lift-off data in LabVIEW.

The system specifications are listed in Table 8.

Table 8. Final system specifications.

Conductivity Range	8 – 100% IACS
Conductivity Accuracy	1.5% IACS
Lift-off Range	0 – 0.6 mm
Lift-off Accuracy	0.04 mm
Weight	21 g
Size	110 × 20 × 15 mm

The presented results validate the proposed measurement system but some improvements in hardware and software are still possible. As such, some of the proposed future work is:

- Include the mini-USB interface in the PCB handler to reduce the system size;
- The system can perform a signal frequency between 1 kHz to 10 MHz, but the conductive and lift-off measure is only calibrated for 60 kHz. An algorithm prepared to frequency variations should be implemented.

REFERENCES

[1] IHS Engineering360, NDT Probes Information, http://www.globalspec.com/learnmore/measurement_test_equipment/nondestructive_test_equipment/specialty_ndt_probes_sensors

[2] Garca-Martín, J.; Gómez-Gil, J.; Vázquez-Sánchez, E. “Non-Destructive Techniques Based on Eddy Current Testing”, Sensors, 11, pp. 2525-2565, 2011.
DOI: 10.3390/s110302525

[3] Placko, D.; Dufour, I., “Eddy current sensors for nondestructive inspection of graphite composite materials”, In Proceedings of the IEEE Conference of the Industry Applications Society (IAS'92), Houston, TX, USA, October 1992. DOI: 10.1109/IAS.1992.244235.

[4] Lion Precision, Eddy-Current Linear Displacement Sensors, http://www.lionprecision.com/eddy-current-sensors/

[5] NDT Resource Center, Complex Impedance Plane, https://www.nde-ed.org/EducationResources/CommunityCollege/EddyCurrents/Instrumentation/impedanceplane.htm

[6] Gui Y. T., Li Y., Mandache C., “Study of lift-off invariance for pulsed eddy-current signals,” IEEE Trans. Magn. 45(1), pp. 184-191, 2009.
DOI: 10.1109/TMAG.2008.2006246

[7] Kriezis E.E., Tsiboukis TD., Panas S.M., Tegopoulost J.A. “Eddy Currents: Theory and Applications”, in Proceedings of the IEEE, 1992, pp 1559 - 1589.
DOI: 10.1109/5.168666

[8] Jack Blitz, Electrical and Magnetic Methods of Non-destructive Testing, Second edition, Springer Science, 1997.
DOI: 10.1007/978-94-011-5818-3

[9] S. Huang and S. Wan. “New Technologies in Electromagnetic Non-destructive Testing”, The Pulsed
Eddy Current Testing, Springer Series in Measurement Science and Technology, 2016.
DOI: 10.1007/978-981-10-0578-7_2